

# Design Optimization of a Triboelectric Energy Harvesting Mechanism for Knee Implants

Alwathiqbellah Ibrahim, Shahrzad Towfighian, and Nael Barakat

**Abstract**—Continuous monitoring of knee implants after total knee replacement (TKR) surgery can play a significant role in increasing the patients' satisfaction rate and extending the lifespan for those implants. The purpose of this study is to optimize the design parameters of the triboelectric energy harvesting mechanism to be embedded in knee implants and act as a battery-less health monitoring sensor. Triboelectric mechanisms convert mechanical energy into electricity, providing both power to operate and information about loads transmitted to the knee from daily life activities. Three different triboelectric energy harvesters were designed and fabricated with different sizes of micro-patterns as design parameters. The harvesters are tested under the simulated walking activity of normal humans. Results show that the harvester with the smaller micro-patterns size is better for energy harvesting. Testing at higher frequencies, all harvesters show an increase in the voltage generated. Moreover, by increasing the amplitude of the applied axial load, a higher voltage is generated. Exploring a different design parameter, which is the harvester's material, and comparing to the previously reported baseline, Titanium-based harvester shows superior from Aluminum-based harvester's performance. Also, a single-degree-of-freedom model is used to model the harvester. Higher applied load results in a higher contact area and more voltage generation. These findings show the promising potential of embedded triboelectric transducers to be utilized as self-powered health monitoring sensors for knee implants and similar applications.

**Index Terms**—TKR, Energy Harvesting, Triboelectric, Knee Implant.

## I. INTRODUCTION

ACTIVITIES of Daily Living (ADL) expose the human knee to most of the body loads. Knee pain is a common complaint that affects people of all ages. Knee pain may be the result of an injury, such as a ruptured ligament or torn cartilage. Medical conditions, including arthritis, gout, and infections, also can cause knee pain. Many types of minor knee pain respond well to self-care measures. Physical therapy and knee braces can also help relieve knee pain. However, in some cases, the knee may require surgical repair. Total Knee Replacement surgery (TKRs) is an effective treatment procedure that can reduce knee pain and improve the ability to move. The increment

Manuscript received January 13, 2021; revised June 13, 2021. This research has been supported by the National Institute of Arthritis and Musculoskeletal and Skin Diseases of the National Institute of Health under award number R21AR068572. The content is solely the authors' responsibility and does not necessarily represent the official views of the National Institute of Health.

Alwathiqbellah Ibrahim (Corresponding author) is an Assistant Professor of Mechanical Engineering Department, University of Texas at Tyler, Tyler, TX 75799 USA, (e-mail: aibrahim@uttyler.edu).

Nael Barakat is a Professor of Mechanical Engineering Department, University of Texas at Tyler, Tyler, TX 75799 USA, (e-mail: nbarakat@uttyler.edu).

Shahrzad Towfighian is an Associate Professor of Mechanical Engineering Department, Binghamton University, 4400 Vestal Pkwy E, Binghamton, NY 13902 USA, (e-mail: stowfigh@binghamton.edu).

in the number of TKR surgeries requires optimization in the implant designs to achieve better performance. However, the lack of information for post operations spurs the researchers to design load monitoring devices for post-operation data. Such information can help estimate the complications that follow the surgery and improve future designs. Nevertheless, the continuous powering of those health monitoring devices continues to be a challenge.

To solve this problem, different attempts have been proposed to address the powering issue. One major solution reported in the literature is based on piezoelectric energy harvesting mechanism [1]–[7]. The first self-powered instrumented TKR attempt was reported by D'Lima et al. [8], [9] in 2006. The mechanism consisted of a coil around the knee. This coil was found to be inconvenient for the patients. Platt et al. [10] proposed an orthopedic implant to generate electrical energy using embedded piezoelectric ceramics in the tibial implant. However, the high thickness of the PZT element required removing a significant amount of the tibial bone during TKR surgery. Later, extensive in vivo studies were reported to measure the loading of the knee joints during daily living activities by the Bergmann group [11]–[13]. They provided complete details about the forces and moments acting on the knee joints. However, their work's major drawback was that the reported data was measured for a specific implant design and cannot be transferred directly to other implants or the natural human knee. The use of sensors for intra-and postoperative estimation has created much enthusiasm for biomedical research in recent years, particularly in the field of orthopedics. Such intra-operative sensors are available commercially for total knee replacements. However, they only help provide data in the operating room and should be removed by the end of the surgery [14]–[16], and the postoperative measurements are missing. Consequently, other issues have come into the picture with this method. In general, piezoelectric energy harvesters have some drawbacks, such as the relatively higher cost of the piezoelectric materials and applications' difficulty in harsh environments. The smaller size and the biocompatibility issues continue to be the biggest challenges in implanted piezoelectric harvesters.

A more recent technique has been reported to show promising results in converting mechanical energy into electricity based on triboelectrification and electrostatic induction [17]–[22]. This new mechanism has attracted significant attention in the research community because of its design simplicity, high energy conversion efficiency, wide material spectrum, low cost, easy fabrication, and wide applications [23]. The triboelectric mechanism requires an insulator that, under repeated rubbing with other appropriate

material with the opposite tendency to lose and gain electrons, will generate electricity [23]–[25]. Under applied dynamic pressure, charges are generated from the friction of the two contact surfaces. The interaction between selected micro-patterns on the surfaces causes an increase of the contact area, which significantly enhances the harvester’s output. This property makes triboelectric harvesters suitable for a knee implant because of the large amplitude of forces available.

The triboelectric effect is characterized by transferring electrons inductively from one material to another when they come in and out of contact. It occurs due to the affinity difference to gain or lose electrons [23], [24]. Due to its advantages such as biocompatibility, high efficiency, low fabrication costs, and lightweight, the triboelectric generator has been used recently in wide energy harvesting applications [29], [30]. The feasibility of the triboelectric energy harvester in powering electronic circuitry for load sensing has been tested and reported in the literature with relatively high efficiency [31]. When the harvester is subjected to cyclic loading, the triboelectric harvester generates a voltage signal dependent on the harvester’s design parameters. These parameters include the gap size between the mating parts, the thickness of the harvester’s material, and external resistance, to name a few. These parameters are designed and configured to fit the harvester in a TKR to monitor the knee loads [32]. The estimation of the knee loads by the triboelectric generator can help determine the wear in polyethylene, stress distribution in the implant and the implant-bone interface, and the stress transferred to the underlying bone [33].

This paper presents the results of an experimental investigation into the effect of design parameters optimization of the triboelectric harvester, such as surface micro-pattern size and configuration, and material selection, on the output voltage generated through triboelectricity under a simplified equivalent gait load, with the intent of using this energy harvesting mechanism in TKR applications. A single-degree-of-freedom system with a piecewise function is used to model the contact and release modes and voltage estimations under different loading conditions. The results can be adapted for further optimization and information collection for high implant performance in future health monitoring systems designs. In addition, this study will be considered the base for further investigation of triboelectric energy harvesting applications for load monitoring in total knee replacement.

II. APPLICATION

The instrumented knee implant is shown in Fig. 1, where it consists of the femur and femoral components, the tibia and tibial tray, the Ultra-high-molecular-weight polyethylene (UHMWPE), and the triboelectric energy harvesters. The triboelectric energy harvesters are placed at the center of the medial and lateral positions between the tibial tray and the UHMWPE bearing, as shown in Fig. 1. The total axial load will be distributed to the medial and lateral parts under walking activity at different load ratios that are proportional to the voltage generated from the two locations.

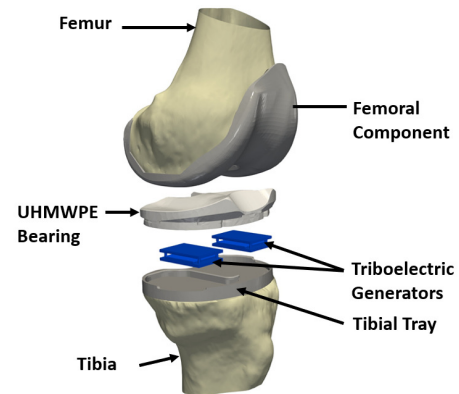


Fig. 1: Schematic of the triboelectric energy harvester configuration.

III. METHODOLOGY

Three triboelectric energy harvesters were designed and built with different parameters as shown in Fig. 2. Each generator consists of two major parts: the upper part, which is made of Titanium with a micro-pattern, and the lower part, made of Polydimethylsiloxane (PDMS) insulator material fabricated using the upper Titanium layer as mold and bonded to a thin aluminum layer. Both Titanium and PDMS material is reported as biocompatible material and hence are suitable for TKR [26]. The shaded area represents the area with micro-patterns. A 3D-printing technology was used to create multiple Titanium molds with micro-patterns of saw teeth made with 300  $\mu\text{m}$  and 100  $\mu\text{m}$  sizes. Because of the limitations of 3D-printing technology, printing molds with smaller micro-patterns size was difficult. To overcome this issue, an Al mold with 25  $\mu\text{m}$  was made through CNC machining. The microscopic pictures for the three molds are shown in Fig. 3a, while the corresponding SEM images for the fabricated PDMS layers are shown in Fig. 3b.

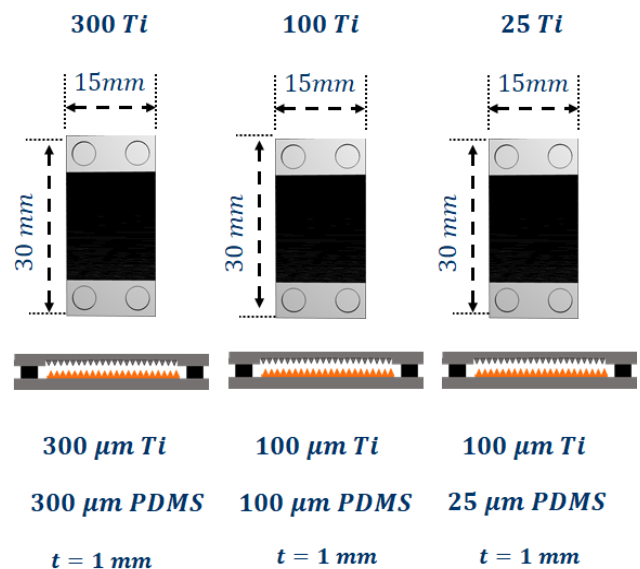


Fig. 2: Schematic of the triboelectric energy harvester configuration.

Four rubber springs at the corners are used to separate the generator layers by 0.5 mm. The rubber springs will create a mechanical restoring force that will maintain a contact and separation motion between the two layers under normal walking activity of daily living. The walking activity will

transfer an axial load to the triboelectric energy harvester through a tibial tray.

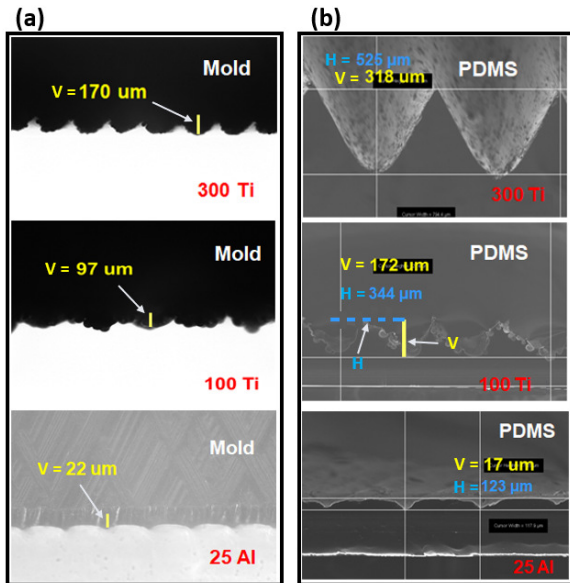


Fig. 3: (a) Microscopic images for the 300 μm, 100 μm Ti, and the 25 μm Al molds, (b) SEM images for the PDMS made using 300 μm and 100 μm Ti molds. The dashed horizontal line is the distance between teeth peaks and labeled with (H) letter, while the solid vertical line is the saw depth and labeled with (V) letter.

#### IV. WORKING MECHANISM

The cyclic contact and separation motion will result in an interaction between the micro-patterns in the two layers of the triboelectric generator. The working mechanism is schematically illustrated on the combination of contact triboelectrification and electrostatic induction, shown in Fig. 4. Initially, the two electrodes are separated from each other and no charge exists, as shown in Fig. 4a. When the axial force is transferred to the knee, the upper Titanium layer contacts the PDMS insulator, and charges would transfer from the PDMS layer due to a higher surface electron affinity, shown in Fig. 4b. Once a relative separation occurs between the Titanium and the PDMS layers, the negative charges on the surface of the PDMS will induce positive charges on the Aluminum electrode to compensate for the triboelectric charges, driving free electrons to flow from the Aluminum to the Titanium, as seen in Fig. 4c.

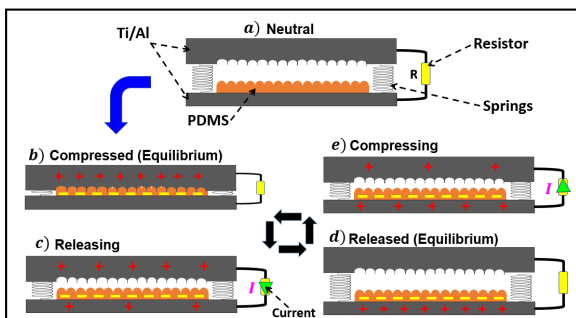


Fig. 4: Operating mechanism for the triboelectric energy harvester.

This electrostatic induction process can generate an output voltage/current signal. When the negative triboelectric charges on the PDMS layer are completely balanced by the

induced positive charges on the Aluminum electrode, no output signals were produced, shown by Fig. 4d. When Titanium approaches the PDMS layer, the induced positive charges on the Aluminum electrode decrease, causing the electrons to flow from the Titanium to the Aluminum electrode until the PDMS layer becomes fully in contact with each other again, resulting in a reversed output signal, as in Fig. 4e. This is a full cycle of the electricity generation process for the triboelectric generator. With a periodical touch on the PDMS layer, an alternating electricity output can be continuously generated. The larger the axial force transferred to the knee, the more power will be generated.

#### V. EXPERIMENTAL SETUP

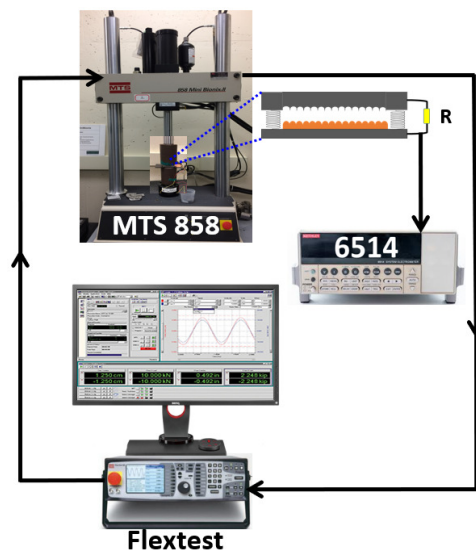


Fig. 5: Experimental setup including a zoomed view for the generator.

A Material testing system (MTS), MTS 858 mini bionix II servohydraulic test system, was used to test the different triboelectric energy harvesters and estimate their range power output. Since the back of the UHMWPE bearing and tibial tray in TKR is flat, as an approximation, the triboelectric generators are placed between two flat cylinders. Furthermore, the normal walking activity is simplified as a uniform half-sine wave at 1 Hz. The MTS machine transfers the axial load to a triboelectric generator placed on top of the lower stationary cylinder attached to a load cell, simulating gait motion. The generated voltage signal is measured through external load resistance using the Keithley M6514 electrometer and ExceLINUX4a corresponding software. A schematic of the experimental setup showing all tools used in this experiment is shown in Fig. 5.

#### VI. EXPERIMENTAL RESULTS AND DISCUSSION

The three fabricated TEG were experimentally tested using the previously mentioned experimental setup under equivalent walking gait load to check the effect of the design parameters on the generator's performance in terms of generated power quantity and range, as well as acting as a load sensor. The walking gait load was approximated as a sine-wave and applied to the generators at different amplitudes and frequencies. The first test included exposing the TEGs to the

same conditions. This allowed the exploration of the effect of the micro-pattern size on the generated output voltage signal. A constant load of 600 N at 1 Hz and a constant external resistance of 22 MΩ were applied to each generator using the MTS machine. The generated voltage was measured using a Keithley 6514 system electrometer. Fig. 6 shows the generated voltage signals for the three generators. The 25 Ti generator with the smallest pattern size generates the highest output voltage. These results were expected because the smaller pattern size will result in a higher surface area of contact between the mold and the PDMS layers, and hence, higher output voltage.

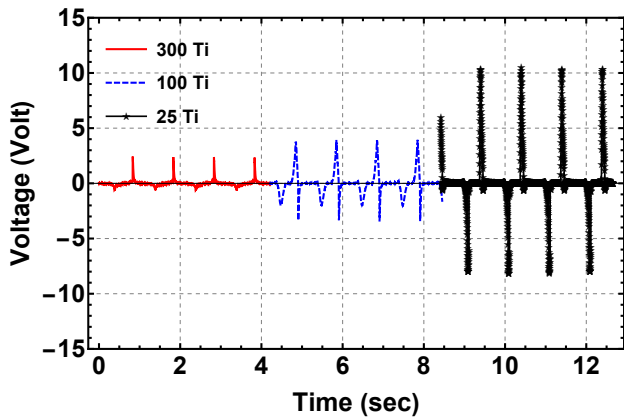


Fig. 6: The generated voltage from the three TEGs at 600 N, 1 Hz, and constant external resistance of 22 MΩ. Smaller pattern size shows higher voltage outputs.

The second test included exposing the TEGs to changing frequency of the equivalent gait load while reserving the previous test conditions and changing the input frequency to 1 Hz, 3 Hz, and 5 Hz. Fig. 7 shows the effect of varying the gait frequency on the output voltage for the three generators, where higher frequencies show higher generated voltages. This can be related to the fact that higher frequencies correspond to more periodic contact and separation between the generator layers. In addition to the previous results, the effect of the pattern size is also confirmed at higher frequencies, i.e., 3 Hz and 5 Hz, where the generated voltage from the 25 Ti generator, as in Fig. 9, has the maximum output voltage compared to the 300 Ti and 100 Ti generators outputs, in Fig. 7 and 8.

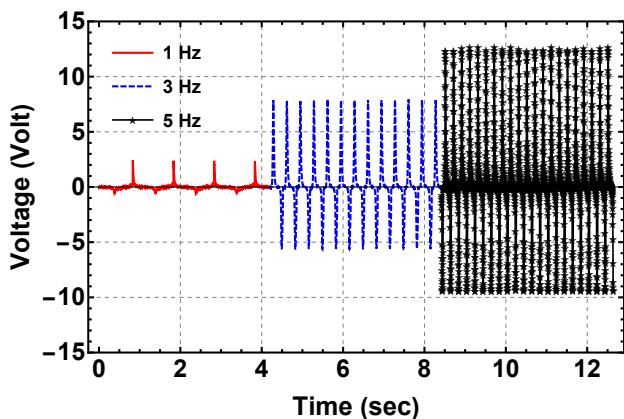


Fig. 7: The generated voltage from the 300 μm TEG at 600 N, 22 MΩ, and at different gait frequencies.

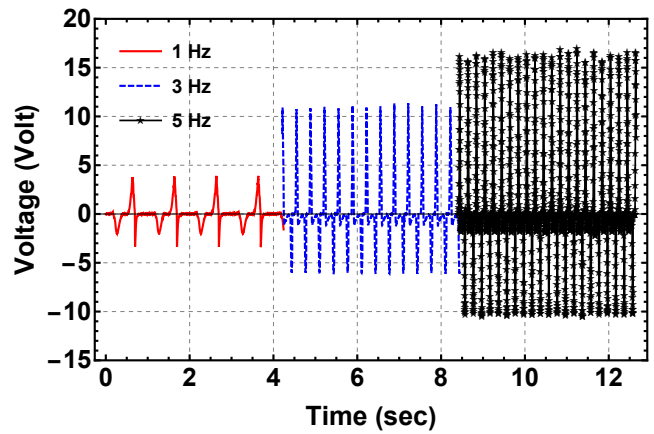


Fig. 8: The generated voltage from the 100 μm TEG at 600 N, 22 MΩ, and at different gait frequencies.

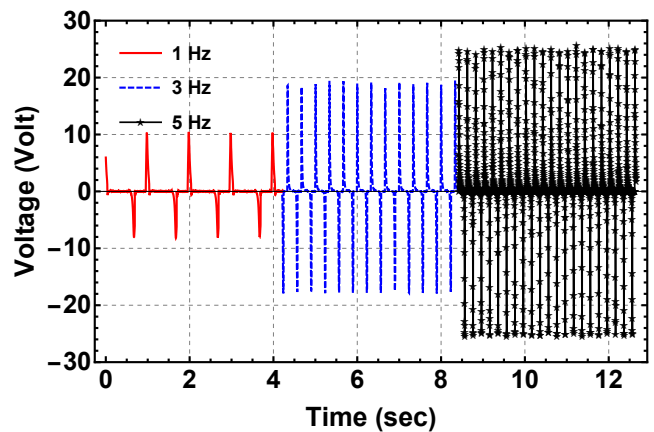


Fig. 9: The generated voltage from the 25 μm TEG at 600 N, 22 MΩ, and at different gait frequencies.

To estimate the enhancement achieved from the new generators compared to our previous prototype generator reported in [27], the 100 Ti generator was selected to be tested since this generator shares the same pattern size of 100 μm with the reported Al TEG [27]. However, the previous prototype had a five times higher area than the 100 Ti. To make the comparison valid, the outputs of the prototype should be divided by unit area. Toward this, the 100 Ti is tested under different gait loads up to 900 N at 1 Hz and at the optimal resistance for the prototype, equivalent to 58 MΩ. Fig. 10 shows the output voltages from 100 Ti at different gait loads compared to the outputs of the previous design at the same loads. The generated voltage from both generators for lower loads is very close in value. However, increasing the gait load above 300 N shows that higher outputs are generated from the 100 Ti compared to Al. It is worth mentioning that the results from the previous design were achieved at the optimal resistance of that generator, 58 MΩ, which may or may not be the optimal resistance for the 100 Ti generator. However, for both cases, the 100 Ti proves that better performance can be achieved than the previous design. Therefore, in addition to the biocompatibility of the Titanium material over the Aluminum in joint replacements, the Titanium-based harvester shows superior performance over the Aluminum-based harvester's performance.

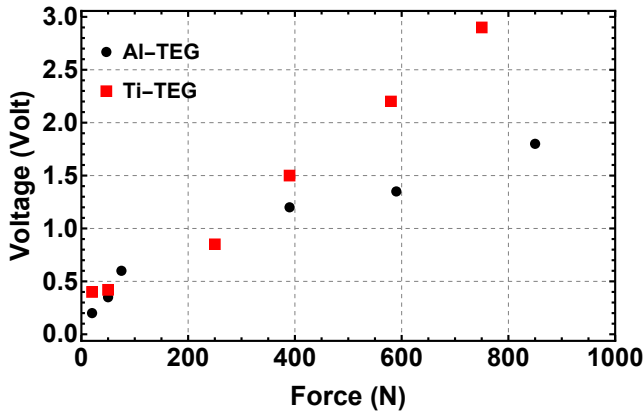


Fig. 10: A comparison between the outputs of the prototype and the 100 *Ti* generators at 1 Hz, 58 MΩ resistance, and at different gait loads. 100 *Ti* shows better performance than the prototype generator.

## VII. THEORETICAL MODEL

The rubber springs will hold the upper electrode. When the system undergoes a vertical load, the upper electrode will be displaced toward the PDMS layer. When the applied load is removed, the springs will return the upper electrode to its original position. When the applied load becomes cyclic, a contact and separation motion between the two layers will be created, and a charge electrification generation will occur. The upper and lower electrodes of the triboelectric generator are simplified to act as a parallel plate capacitor. Two electrical fields are generated, one at the PDMS layer and one at the air gap between the two electrodes. According to this, the electrical equation that governs the output voltage is given by:

$$\dot{q}(t) = -\frac{q(t)}{R\epsilon_0 S_{max}} \left( \frac{T}{\epsilon_r} - y(t) \right) + \frac{\sigma S(F)}{R\epsilon_0 S_{max}} y(t) \quad (1)$$

Where  $q(t)$  is the number of transferred charges between the two electrodes,  $S_{max}$  is the maximum area of contact based on the generator layers dimensions.  $S(F)$  is the surface area of contact under contact separation motion.  $R$  is the resistance, and  $T$  is the thickness of the PDMS layer.  $\epsilon_0 = 8.85 * 10^{12}$  F/m is the vacuum permittivity,  $\epsilon_r$  is the dielectric constant of the PDMS, and  $\sigma$  is the surface charge density. The contact-separation motion between the harvester electrodes can be modeled as a single-degree-of-freedom system with a piecewise function to model the contact and release modes and estimate produced voltage. According to Fig. 4, the upper layer will start to displace under an applied force and start to penetrate inside the PDMS layer. Accordingly, the displacement of the springs will increase proportionally to the increased applied force. Experimentally, the upper layer will undergo a half-sine waveform as shown in the normalized displacement, Fig. 11. The experimental displacement can be represented mathematically by the following piecewise form:

$$y(t) = \begin{cases} Y_{max} \Psi(t), & y(t) \leq 0 \\ 0, & y(t) > 0 \end{cases} \quad (2)$$

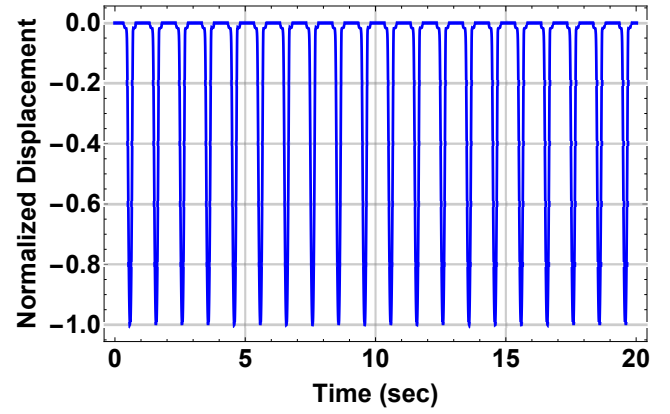


Fig. 11: Half-sine wave normalized displacement.

Where  $\Psi(t)$  is the normalized displacement function at 1 Hz motion matching regular human walking motion.  $Y_{max}$  is the maximum possible penetration of the upper layer in the PDMS layer, which is assumed to be 90% of the total PDMS thickness. A representation of this displacement is shown in Fig. 12.

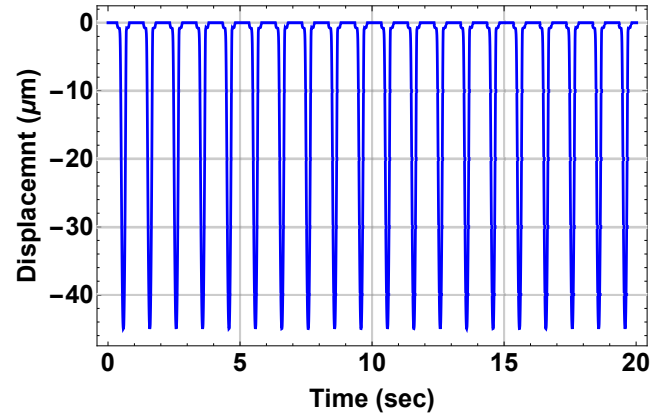


Fig. 12: Maximum possible penetration of the harvester's upper layer in the PDMS layer.

The surface charge density is a function of multiple factors, such as the materials' chemical properties and the micro-surface patterns that control the area of contact [28]. Therefore, to counter this variability in the model, the surface charge density is assumed to have a similar form to the normalized displacement wave and be a function of the applied force  $F$  and time as shown below:

$$\sigma(F, t) = 1 * 10^{-9} * F * \Psi(t) \quad (3)$$

The voltage produced by the generator is the total voltage produced in the air gap and the PDMS layer. By solving equations 1-3 using the parameters on Table. I, we can estimate the voltage signal produced at any applied force. At the beginning, we will investigate the effect of the applied load on the amount of voltage generated. Toward this, the maximum area of contact,  $S_{max}$ , and the surface area of contact,  $S(F)$ , are assumed to be equal and cancel each other in the last term of Eq. 1. Fig. 13 shows the generated voltage signal resulting from applying 100 N cyclic loads. The maximum output voltage of 4.4 V is generated.

TABLE I: Parameters used in the model.

Parameters		Value
Forcing Frequency	$\Omega$	1 Hz
PDMS Thickness	$T$	50 $\mu\text{m}$
Permeability of free space	$\epsilon_0$	$8.85 * 10^{12}$ F/m
Permeability of PDMS	$\epsilon_r$	3.4 F/m
Resistance	$R$	22 M $\Omega$

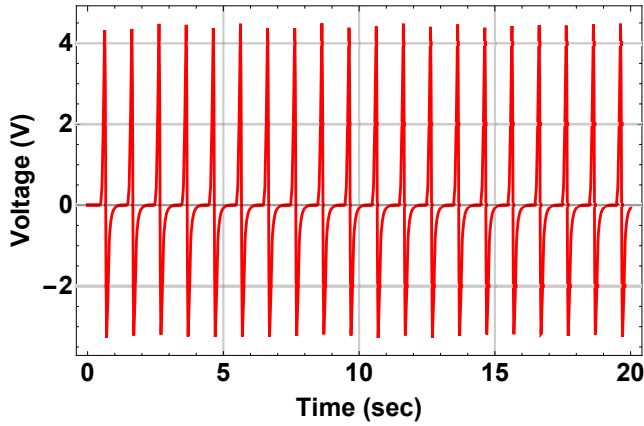


Fig. 13: Simulated voltage output from the TKR triboelectric generator at an applied load of 100 N.

Increasing the applied load amplitude to 600 N results in a significant increase in the generated voltage signal shown in Figure 14, where the maximum output voltage reaches 26.8 V.

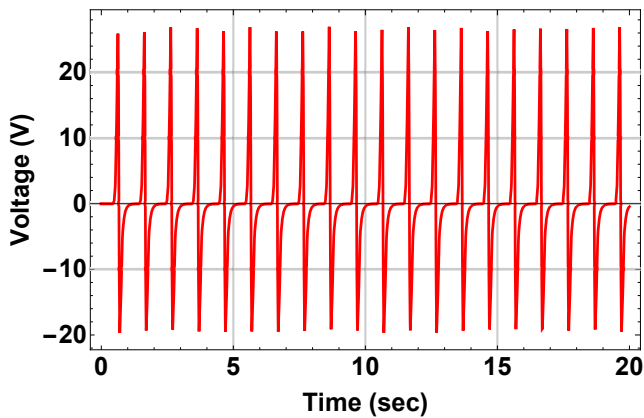


Fig. 14: Simulated voltage output from the TKR triboelectric generator at an applied load of 600 N.

To investigate the effect of the contact area, the surface charge density is assumed to be constant of  $5.5 * 10^{-7}$ , while the surface area of contact,  $S(F)$ , is assumed to be variable and function of the applied force and given by Eqn.4:

$$S(F) = 3.1 * 10^{-7} * F \quad (4)$$

The voltage generated under 100 N is shown in Fig. 15, where a 2.4 V generated voltage is achieved. By increasing the applied load to 600 N, the generated voltage amplitude reaches a higher value of 14.6 V, Fig. 16. The higher generated voltage at the higher applied load is because more penetration of the upper layer inside the PDMS layer results in more accumulated charges. These outcomes show that triboelectric energy harvester is a function of different

parameters that can significantly affect the amount of energy harvested. Furthermore, these findings open the door for optimization studies to achieve high-performance triboelectric energy harvesters.

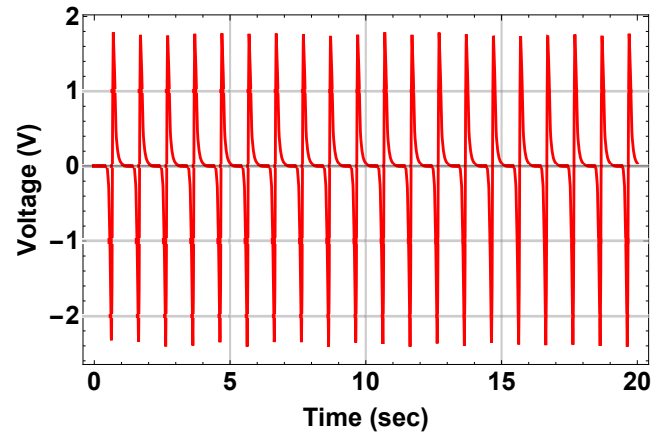


Fig. 15: Simulated voltage output from the TKR triboelectric generator with variable surface area of contact and at an applied load of 100 N.

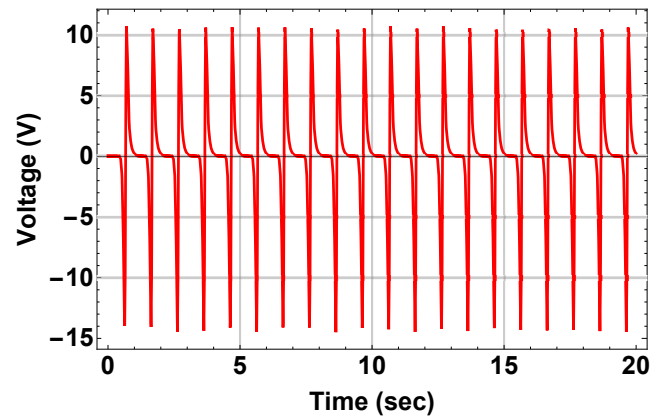


Fig. 16: Simulated voltage output from the TKR triboelectric generator with variable surface area of contact and at an applied load of 600 N.

## VIII. CONCLUSION

Experimental investigation of design parameters on triboelectric energy harvesters for load measurements of TKR was conducted using three different TEGs. The harvesters were tested under simplified equivalent axial gait loads using an MTS machine. The harvester with the smallest pattern size of 25  $\mu\text{m}$  shows the highest output generated. Also, frequency and load effects on the generated voltage were examined. Higher voltage output was generated by increasing the applied load. The proportionality of the generated voltage to the applied load shows a promising concept for employing the triboelectric energy harvester mechanism for load sensing in TKR. In addition, a theoretical single-degree-of-freedom model is presented, where the effect of the applied loads and surface area of contact is explored. Higher applied load results in a higher contact area and more voltage was generated. Furthermore, the biocompatible Titanium-based harvester shows a better performance than the Aluminium-based harvester, opening the door to optimizing the load sensor for the TKR.

## REFERENCES

- [1] Wang, Zhong Lin, and Jinhui Song. "Piezoelectric Nanogenerators Based on Zinc Oxide Nanowire Arrays." *Science* 312.5771 (2006): 242-246.
- [2] Cheng, Xiaoliang, et al. "Implantable and Self-Powered Blood Pressure Monitoring Based on a Piezoelectric Thinfilm: Simulated, in Vitro and in Vivo Studies." *Nano Energy* 22 (2016): 453-460.
- [3] Pi, Zhaoyang, ET al. "Flexible Piezoelectric Nanogenerator Made of Poly (Vinylidene fluoride-Co-Trifluoroethylene)(Pvdf-Trfe) Thin Film." *Nano Energy* 7 (2014): 33-41.
- [4] Zhu, Guang, et al. "Flexible High-Output Nanogenerator Based on Lateral Zno Nanowire Array." *Nano Letters* 10.8 (2010): 3151-3155.
- [5] Park, Kwi-IL, et al. "Flexible Nanocomposite Generator Made of batio3 Nanoparticles and Graphitic Carbons." *Advanced Materials* 24.22 (2012): 2999-3004.
- [6] Kwon, Junggou, et al. "A High Performance Pzt Ribbon-Based Nanogenerator Using Graphene Transparent Electrodes." *Energy Environmental Science* 5.10 (2012): 8970-8975.
- [7] Hwang, Geon-Tae, et al. "Self-Powered Cardiac Pacemaker Enabled by Flexible Single Crystalline Pmn-PT Piezoelectric Energy Harvester." *Advanced Materials* 26.28 (2014): 4880-4887.
- [8] D'Lima, Darryl D., et al. "Tibial Forces Measured in Vivo After Total Knee Arthroplasty." *the Journal of Arthroplasty* 21.2 (2006): 255-262.
- [9] D'Lima, Darryl D., et al. "In Vivo Knee Moments and Shear After Total Knee Arthroplasty." *Journal of Biomechanics* 40 (2007): S11-s17.
- [10] Platt, Stephen R., et al. "The Use of Piezoelectric Ceramics for Electric Power Generation Within Orthopedic Implants." *Ieee/Asme Transactions on Mechatronics* 10.4 (2005): 455-461.
- [11] Kutzner, I., et al. "Loading of the Knee Joint During Activities of Daily Living Measured in Vivo in Five Subjects." *Journal of Biomechanics* 43.11 (2010): 2164-2173.
- [12] Kutzner, Ines, et al. "Knee Adduction Moment and Medial Contact Force—Facts About Their Correlation During Gait." *Plos One* 8.12 (2013): E81036.
- [13] Bergmann, Georg, et al. "Standardized Loads Acting in Knee Implants." *Plos One* 9.1 (2014): E86035.
- [14] Meneghini, Robert M., et al. "Can Intraoperative Sensors Determine the "Target" Ligament Balance? Early Outcomes in Total Knee Arthroplasty." *the Journal of Arthroplasty* 31.10 (2016): 2181-2187.
- [15] Gustke, Kenneth a., et al. "A New Method for Defining Balance: Promising Short-Term Clinical Outcomes of Sensor-Guided Tka." *the Journal of Arthroplasty* 29.5 (2014): 955-960.
- [16] Roche, Martin, Leah Elson, and Christopher Anderson. "Dynamic Soft Tissue Balancing in Total Knee Arthroplasty." *Orthopedic Clinics* 45.2 (2014): 157-165.
- [17] Zhu, Zhiyuan, et al. "Based Methodology for Investigation of Triboelectric Nanogenerators." *Energy Reports* 5 (2019): 393-397.
- [18] Fan, Feng-RU, Zhong-Qun Tian, and Zhong Lin Wang. "Flexible Triboelectric Generator." *Nano Energy* 1.2 (2012): 328-334.
- [19] Wang, Zhong Lin. "Triboelectric Nanogenerators as New Energy Technology for Self-Powered Systems and as Active Mechanical and Chemical Sensors." *Acs Nano* 7.11 (2013): 9533-9557.
- [20] Shaukat, Rayyan Ali, et al. "Bio-Waste Sunflower Husks Powder Based Recycled Triboelectric Nanogenerator for Energy Harvesting." *Energy Reports* 7 (2021): 724-731.
- [21] Atmeh, Mohammad, et al. "Performance Analysis of Triboelectric Energy Harvester Designs for Knee Implants." *Health Monitoring of Structural and Biological Systems XV. Vol. 11593. International Society for Optics and Photonics, 2021.*
- [22] Davis, James, et al. "Design and performance simulation of a triboelectric energy harvester for total hip replacement implants." *Health Monitoring of Structural and Biological Systems XV. Vol. 11593. International Society for Optics and Photonics, 2021.*
- [23] Wang, Zhong Lin. "Triboelectric Nanogenerators as New Energy Technology and Self-Powered Sensors—Principles, Problems and Perspectives." *Faraday Discussions* 176 (2015): 447-458.
- [24] Zi, Yunlong, et al. "Effective Energy Storage From a Triboelectric Nanogenerator." *Nature Communications* 7.1 (2016): 1-8.
- [25] Ibrahim, Alwathiqbellah, Abdallah Ramini, and Shahrzad Towfighian. "Triboelectric Energy Harvester With Large Bandwidth Under Harmonic and Random Excitations." *Energy Reports* 6 (2020): 2490-2502.
- [26] Bélanger, Marie-Claire, and Yves Marois. "Hemocompatibility, Biocompatibility, Inflammatory and in Vivo Studies of Primary Reference Materials Low-Density Polyethylene and Polydimethylsiloxane: A Review." *Journal of Biomedical Materials Research: An Official Journal of the Society for Biomaterials, the Japanese Society for Biomaterials, and the Australian Society for Biomaterials and the Korean Society for Biomaterials* 58.5 (2001): 467-477.
- [27] Ibrahim, Alwathiqbellah, et al. "A Smart Knee Implant Using Triboelectric Energy Harvesters." *Smart Materials and Structures* 28.2 (2019): 025040.
- [28] Henniker, J. "Triboelectricity in Polymers." *Nature* 196.4853 (1962): 474-474.
- [29] Fan, Feng-RU, Zhong-Qun Tian, and Zhong Lin Wang. "Flexible Triboelectric Generator." *Nano Energy* 1.2 (2012): 328-334.
- [30] Wang, Zhong Lin. "Triboelectric Nanogenerators as New Energy Technology for Self-Powered Systems and as Active Mechanical and Chemical Sensors." *Acs Nano* 7.11 (2013): 9533-9557.
- [31] Ibrahim, Alwathiqbellah, et al. "Feasibility of Triboelectric Energy Harvesting and Load Sensing in Total Knee Replacement." *Asme 2018 Conference on Smart Materials, Adaptive Structures and Intelligent Systems. American Society of Mechanical Engineers Digital Collection, 2018.*
- [32] Ibrahim, Alwathiqbellah, et al. "Parametric Study of a Triboelectric Transducer in Total Knee Replacement Application." *Journal of Intelligent Material Systems and Structures* 32.1 (2021): 16-28.
- [33] Ibrahim, Alwathiqbellah, et al. "Analysis of a Triboelectric Energy Harvester for Total Knee Replacements Under Gait Loading." *Active and Passive Smart Structures and Integrated Systems XIII. Vol. 10967. International Society for Optics and Photonics, 2019.*